Optimization of a Vision-Based SHM System for Imaging Subsurface Impact Damage in Composite Structures

T. BRYCE ABBOTT and FUH-GWO YUAN

ABSTRACT

This paper describes the optimization of a computer vision-based technique for visualizing subsurface barely visible impact damage (BVID) in composite structures. The system uses a piezoshaker for exciting a guided wavefield with a sweeping frequency in the near-ultrasonic frequency range, a digital camera or stereo-camera for recording surface dynamics, and an energy-based damage imaging condition for identifying local resonance from standing waves within damage regions. The method for extracting surface dynamics from the videos was optimized, evolving through three techniques – 3D digital image correlation (DIC), off-axis 2D DIC, and image decorrelation – with the ultimate goal of creating a practical and efficient vision-based method for BVID inspection. Each proposed technique was applied to inspect two CFRP composite-honeycomb panels that had been subjected to low-velocity impacts. Damage images produced with all techniques for a 100-mm ξ 100-mm FOV using a three-second video show accurate damage imaging ability. The processing time required by the optimized decorrelation technique for extracting surface dynamics is approximately 15 times less than 3D DIC and 5 times less than off-axis 2D DIC. The increased efficiency, reduced complexity, and demonstrated accuracy of the system suggests a high potential for practical baseline-free and in-time computer-vision-based structural health monitoring (SHM) and baseline-free subsurface damage imaging for critical composite structures.

INTRODUCTION

Carbon fiber reinforced polymer (CFRP) composites and composite honeycomb structures have received wide acceptance for use in lightweight structures in the aerospace and automotive industry; however, with their adoption comes unique challenges for inspection. Compared to metallic alloys, composites are much more vulnerable to impact damage due to the brittle behavior of the matrix and low through-thickness strength [1]. Low-velocity impacts can create sub-surface damage,

North Carolina State University, Department of Mechanical and Aerospace Engineering, 1840 Entrepreneur Drive, Raleigh, NC 27606, U.S.A.

typically in the form of layer delamination and matrix cracking, which can significantly reduce structural integrity while leaving little evidence on the surface [2, 3]. This type of damage, known as barely visible impact damage (BVID), poses a significant challenge for ensuring vehicle safety since traditional visual inspection techniques cannot confidently detect this damage. Thus, more robust non-destructive inspection (NDI) and structural health monitoring (SHM) methods are needed to ensure safety and reduce inspection time and costs.

With the aim of ensuring the safety and serviceability of structures in a practical manner to supplement or replace visual inspection, computer vision techniques have been explored, which rely on image processing algorithms to extract meaningful information from images automatically and objectively [4,5]. In contrast with other sensing methods for SHM, digital cameras can sense the entire region of interest (ROI) instantaneously with high spatial density since each pixel acts as a sensor.

The continuous advancement of integrated chip technology has enabled computer vision to expand to more complex techniques for local damage detection, like digital image correlation (DIC). DIC is a vision-based technique that is well-established as a tool for non-contact measurement of surface deformations or contours in the field. DIC works by comparing images of the structure's surface, on which a random speckle pattern has been applied, before and after deformation. By matching unique areas of the speckle pattern, called subsets, in the deformed and reference image, the local displacement can be computed. By considering multiple subsets throughout the image, the surface deformation can be obtained across the entire ROI.

Standard DIC techniques can be broadly divided into two categories: 2D DIC and 3D DIC. 2D DIC uses a single fixed camera to capture in-plane displacements of planar surfaces, while 3D DIC uses a stereo pair of cameras to measure all three components of surface displacement (in-plane and out-of-plane) based on triangulation. 3D DIC is generally considered more robust since it can be applied to more-complex geometries and is not limited to in-plane measurements; however, the stereo system is much more complex than the system for 2D DIC and requires a detailed calibration procedure. Additionally, the stereo matching required for 3D DIC increases the processing time required by a factor of approximately three compared to 2D DIC. In addition to the standard DIC techniques, off-axis 2D-DIC exists with

TABLE I: COMPARISON OF IMAGE PROCESSING TECHNIQUES FOR EXTRACTING SURFACE MOVEMENT FROM IMAGES

	3D DIC	**Off-Axis 2D DIC**	**Image Decorrelation**
Extraction Feature	Displacement in all three directions in space (vector)	Displacement in two directions relative to camera in pixels (vector)	Decorrelation magnitude relative to the camera (scalar)
Extraction Method	Shape function matching and triangulation	Shape function matching (with an optical axis oblique to the surface)	Direct comparison of matching pixel groups (with an optical axis oblique to the surface)
Hardware Requirements	Two cameras in a calibrated stereo-system	Single camera	Single camera
Displacement Limits	Can be multiple pixels	Can be multiple pixels	Must be sub-pixel
Computational Complexity	Very high	High	Low
Data Post-Processing Time	Very slow (~30×)	Slow (~10×)	Rapid (~1×)

special applicability, which uses a single camera whose optical axis is oblique to the test sample surface to measure transverse surface displacement [6]. Recent advances and applications of DIC have been reviewed by Pan and Sutton et al. [7,8].

Ultrasonic guided-wave-based techniques for SHM utilize guided (or Lamb) waves for inspection that can propagate long distances across plate-like structures with little attenuation and interact with any discontinuities [9]. By sensing and reconstructing the wavefield, evidence related to the location and shape of any damage within the structure, such as reflections and standing waves, can be extracted with a damage imaging condition to visualize the hidden damage. In 2019 in the authors' lab, a proof of concept for sensing guided waves using DIC to create damage images was demonstrated for the first time [10].

This paper expands on previous work to significantly improve practicality. The most enabling improvement is a total wave energy (TWE) damage imaging condition that is sensitive to the higher wave energy produced by standing waves trapped within damage boundaries [11]. Additional information about this TWE imaging condition can be found in the authors' 2023 publication [11]. This energy-based method does not require the Nyquist sampling condition to be met since wave mode analysis is not required, so relatively low frame rates are sufficient. Also, only the magnitude of surface change between images is of importance, so tracking displacement through subset matching is not necessary.

Decorrelation is a common algorithm associated with computer vision and is often used for defect detection applications involving the quantification of visible irregularities in a current image compared to a reference pristine image [12]. However, a different, non-traditional use for image decorrelation is proposed in this work, which relies on decorrelation to determine the magnitude of change in a

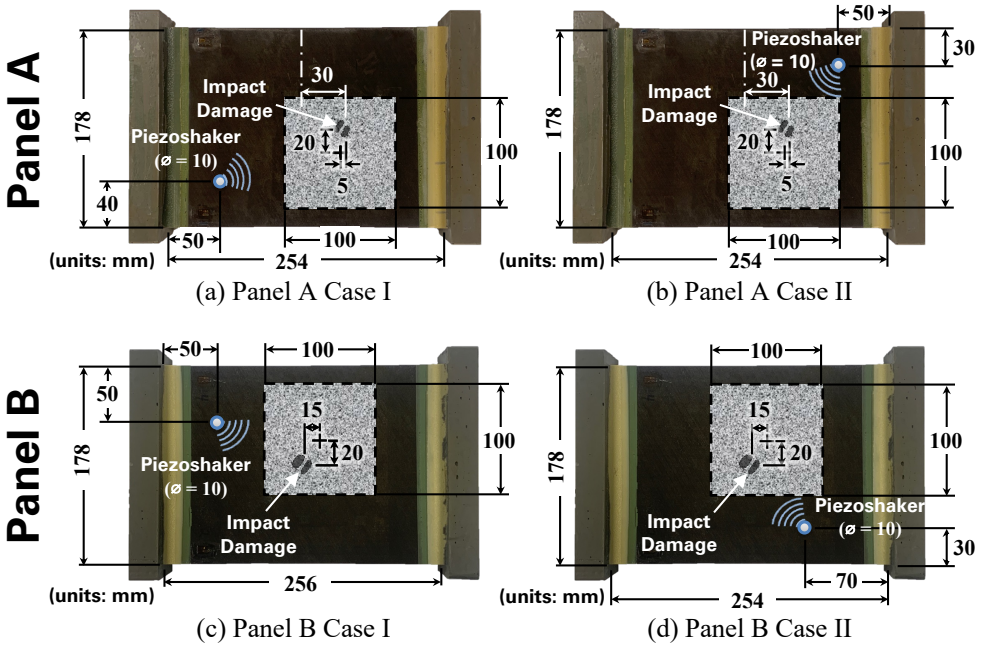

Figure 1. The dimensions and layout of the two composite-honeycomb panels with subsurface BVID used for validation with different piezoshaker locations. The speckled region represents the area covered by the speckle pattern and the field of view (FOV) of the cameras.

structure between a dynamic and static state, proportional to displacement. Like DIC, this method requires a black-and-white speckle pattern to be applied to the surface. Surface movement will shift the speckles, causing a change in the grayscale intensity of the pixels capturing the speckle edges, as long as the movement is subpixel. Decorrelation can quantify this change in an efficient pixel-by-pixel manner, making it a prime candidate for replacing DIC when used with the TWE criterion since it should be sensitive to areas of larger displacement.

This paper describes the optimization of the technique for extracting surface dynamics from images since this step has a large influence on the processing time, sensitivity, and required complexity of the complete damage imaging system. In the next section, the experimental methodology and system components are described in detail. The subsequent sections then follow the steps of system development and optimization: first, 3D DIC for subsurface damage imaging was first attempted to show that standing waves could be captured using white-light imaging [11]; then, off-axis 2D DIC was used to demonstrate that a single camera is sensitive enough for damage imaging; and finally, decorrelation was applied to reduce system complexity, avoid the complex DIC algorithm, and significantly reduce processing time. The advantages and disadvantages of each for this application are discussed in Table I. A comparison of the techniques and comments on the success of the study are finally presented in the conclusion section.

EXPERIMENTAL METHODOLOGY

Two CFRP composite honeycomb panels, shown in Figure 1, were used to demonstrate the proposed technique. Both consist of a 25.4mm-thick aluminum honeycomb core sandwiched between two 6-ply CFRP composite face sheets. Each has in-plane dimensions of 178 mm × 254 mm. Additional details on the panels and their material properties can be found in Leone et al. [13].

To create BVID with which to test the proposed method, each panel was subjected to a controlled, 2-joule impact via a drop tower. This low-velocity impact

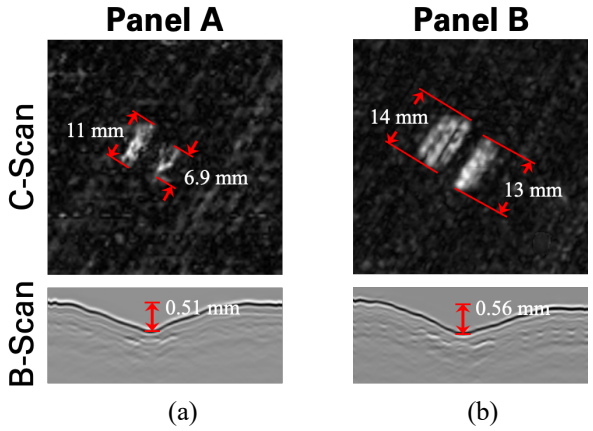

Figure 2. UT scans of the damage located at each impact location on the surface of (a) Panel A and (b) Panel B. The C-scan region shown corresponds to a 50.8 mm × 50.8 mm region centered around the impact location. Below are B-scan images, showing an exaggerated view of the indentations.

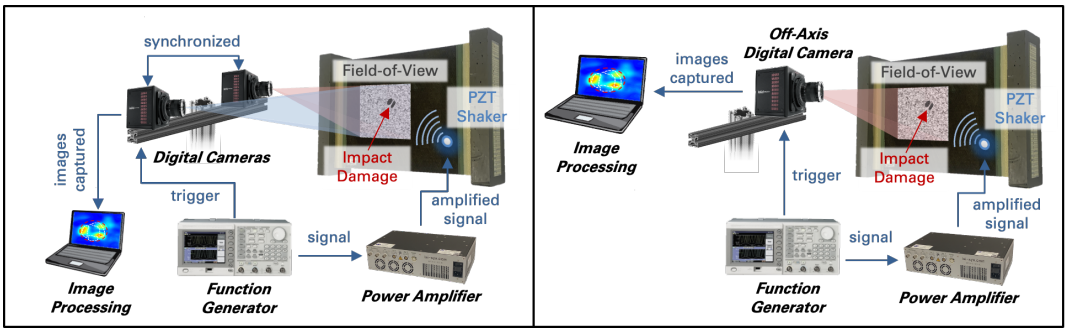

Figure 3. Experimental setup for (a) the stereo-camera system for damage imaging through 3D DIC and (b) the single-camera system for damage imaging through off-axis 2D DIC and decorrelation.

created subsurface damage in the form of delamination. Figure 2 shows ultrasonic C-scan images of the resulting damage in each panel. Though dents were created, these can barely be felt by running a finger over the surface and there is no visual evidence of impact.

With DIC, the uniqueness of each subset is assured by applying a random speckle pattern to the plate over the region of interest. A speckle size that is four times the pixel size was chosen to avoid aliasing [14]. A speckle pattern generator software from Correlated Solutions, Inc. was used to generate a pattern, which was then printed on standard copy paper with a high-resolution (1200 × 2400 dots per inch) laser printer. The paper speckle pattern was carefully applied to the plate with a thin, even layer of white multi-purpose PVA glue. This method provides a quick, temporary, and inexpensive method for speckle application that does not permanently alter the surface. Since the proposed decorrelation technique also requires a black-and-white speckle pattern for quantifying changes based on grayscale intensity shifts, the same speckle pattern used for DIC was also used for decorrelation.

To excite the frequency content necessary to support local resonance in the damage regions of the panels, a high-power isi-sys PS-X-04 piezoshaker was used. This was attached to the surface of the panel on the same side as interrogation using a vacuum suction cup attachment. To promote sonic penetration into the panel, ultrasonic couplant was applied between the piezoshaker element and the panel surface.

A chirp excitation was generated using a Tektronix AFG3022C function generator at 3 ± 2V (unipolar) to provide the necessary frequency content for resonance. This signal was amplified to 120 ± 80V using an isi-sys HPDA-0-180-1C high-power amplifier and sent to the piezoshaker for excitation (Figure 3). A chirp excitation from 10 to 20 kHz over a 3-s period of three seconds was chosen because multiple resonance frequencies were expected to fall within this range for many damage scenarios, supported by laser Doppler vibrometery (LDV) data and finite element analysis (FEA) simulations. A long period of excitation period provided time for energy to accumulate within the damage region and for significant resonance to occur during the sweep when the appropriate frequencies were being excited. The experimental setup is shown in Figure 3.

Photron FASTCAM Mini AX-200 high-speed cameras were used for recording the surface dynamics. The cameras have a maximum resolution of 1024 pixels × 1024

pixels at 6400 frames per second (fps) with a 12-bit depth. The cameras were equipped with Nikon AF-S VR Micro-Nikkor 105mm f/2.8G IF-ED lenses. Three Zaila Daylight light-emitting diode (LED) fixtures were used to provide adequate lighting to accommodate the (1/60000) s shutter time required to minimize blur. The camera(s) and the LED fixtures were mounted to a rigid frame to minimize external vibrations.

For a 1-megapixel resolution, the out-of-plane displacement resolution is approximately 0.00001 of the FOV, though this value is heavily dependent on system setup [15]. When resonance is present, the out-of-plane vibration magnitude is less than 10 microns. From this, a FOV of 100 mm × 100 mm was chosen to maximize the area that can be inspected while maintaining the system's sensitivity to damage.

3D DIC

3D DIC was first explored for BVID inspection in a 2023 paper by the authors to demonstrate the potential of a white-light optical technique for visualizing subsurface BVID through capturing standing waves [8]. 3D DIC was used first since it offers the best sensitivity, as it can fully capture both in-plane and transverse displacement components. This allows it to capture the transverse wave modes (mainly the A_0 wave mode), which are approximately three-times the magnitude of in-plane modes.

In this previous work, 3D DIC was performed after calibration with the stereo-camera setup shown in Figure 3a [11]. Each camera was oriented such that the optical axis of each camera was approximately 8° from the normal and the commercial application, VIC-3D by Correlated Solution, Inc., was used for calibration and 3D DIC. This effectively converted the pixel intensities from stereo-camera videos ($I_M(x,y,t)$; M=left, right) to a 3D surface displacement video ($u(x,y,t)$, $v(x,y,t)$, $w(x,y,t)$). A DIC subset size of 21 × 21 pixels was used with a step size of 7 pixels. Before processing, a high-pass filter with a cutoff frequency of 0.2 kHz was applied to the displacement data to remove ambient noise. While this also may remove some temporally aliased signals near intervals of the sampling rate (6.4 kHz), there should be sufficient opportunities for resonance at other frequencies to still provide a quality damage image since there are many resonance modes.

In MATLAB, the TWE imaging condition was applied, converting the 3D surface displacement video ($u(x,y,t)$, $v(x,y,t)$, $w(x,y,t)$) extracted using 3D DIC to a physical domain, $I(x, y)$, representing the subsurface damage image within the FOV. This TWE condition is based on the monogenic signal, which is obtained via a Reisz transform and used to compute the instantaneous amplitude. The local wave energy is then calculated spatially over time from the instantaneous amplitude. Additional information about this TWE imaging condition can be found in [11]. For 3D DIC, the damage images are the norm of the TWE of each 3D directional velocity component:

$$I_{3D\ DIC}(x,y) \equiv \sqrt{|\mathrm{TWE}_x(x,y)|^2 + \left|\mathrm{TWE}_y(x,y)\right|^2 + |\mathrm{TWE}_Z(x,y)|^2} \qquad (1)$$

For the formulation of the TWE in both DIC cases, the signal is considered the product of the displacement directional component and angular frequency during the

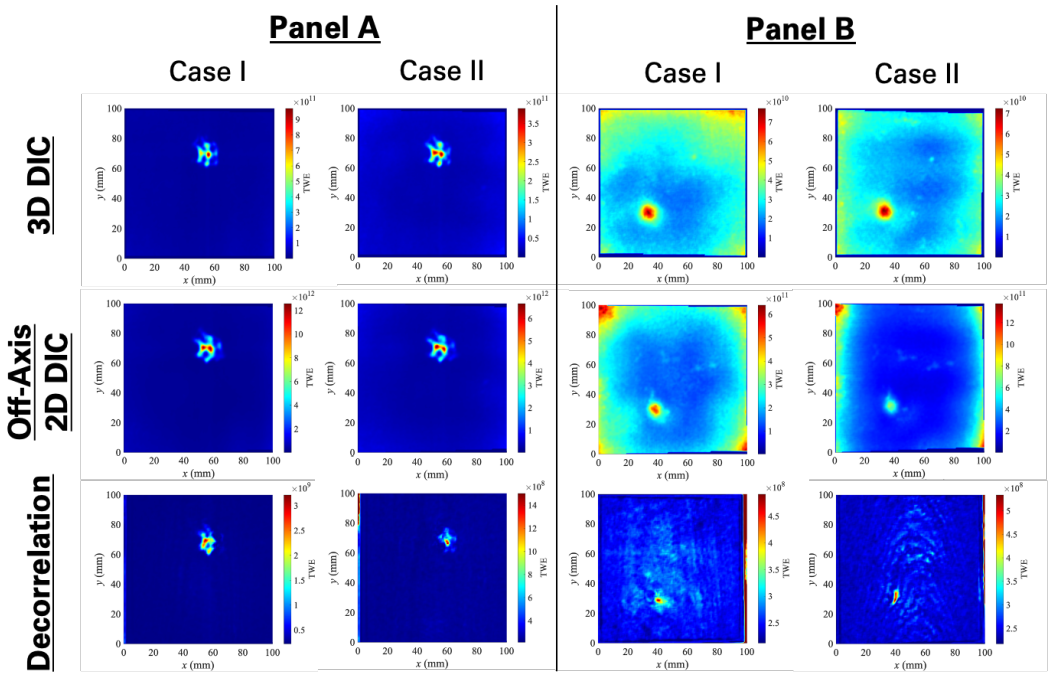

Figure 4. Total wave energy damage images computed using 3D DIC, off-axis 2D DIC, and decorrelation for the two panels and setups described in Figure 1.

frequency sweep to represent the velocity. While the actual velocity could not be derived due to aliasing, this simplified representation of velocity serves the purpose of accounting for frequency since the displacement amplitude is frequency dependent.

The damage imaging results produced from the displacement data extracted using 3D DIC are presented in Figure 4. In both Panel A images, the damage image has more contrast than in the Panel B images. In the Panel B images, artifacts around the left and right edges are present, which are likely caused by a combination of non-uniform lighting and poorer focus from the limited depth of field in these regions. However, the TWE at the damage in Panel B is approximately one order smaller than that of Panel A, so these artifacts are present in Panel A images but not visible due to the scaling. Though each panel was subjected to an impact with the same energy (2-Joules), the subsurface damage was created differently and has different resonance frequencies. Thus, fewer resonance events could have occurred during the 10-20 kHz sweep for Panel B and therefore did not contribute as much to the TWE. It is also possible that significant resonance could have been observed below 0.2 kHz due to aliasing and was attenuated by the high pass filter. Despite the discrepancies in the damage images, the damage in all cases has relatively high contrast and clearly matches the expected damage locations described in Figure 1.

OFF-AXIS 2D DIC

After the 3D DIC technique demonstrated an ability to image BVID in a composite panel using a single 3-second video, off-axis 2D was explored as the next

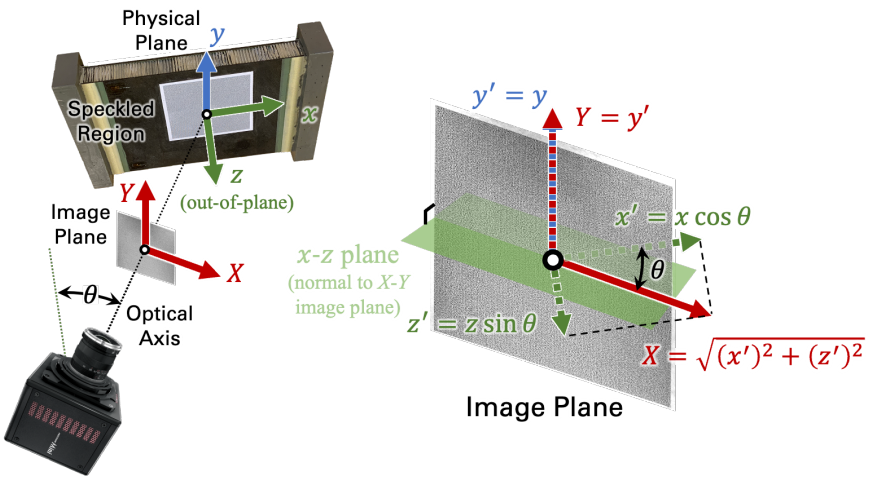

Figure 5. (a) Off-axis single-camera experimental setup where the optical axis is oriented θ degrees around the y-axis with respect to the surface normal and (b) the contribution of surface displacements to the movement observed by the camera. From the image plane (perspective of the camera), the observed movements in the y-direction match the displacements in the physical plane (on the surface), but the observed movements in the x-direction are a combination of x- and z-direction movements of the physical plane.

step in the optimization process to demonstrate the ability of a single camera to capture the local resonance with the sensitivity needed to image BVID. For this, the second camera was removed from the system and calibration was not necessary. The optical axis of the remaining camera was oriented approximately 22° around the y-axis of the panel with respect to the surface normal, integrated with the experimental setup in Figure 3b. With this orientation, the x-displacement perceived by the camera and calculated via 2D DIC does not accurately represent the in-plane x-displacement of the panel; rather, the x-displacement computed via 2D DIC will be the norm of $\cos(\theta)$ of the in-plane x-displacement and $\sin(\theta)$ of the out-of-plane displacement. For an angle of $\theta = 22°$, 92.7% of the in-plane x-displacement will be observed and 37.5% of the out-of-plane z-displacement will be observed. Figure 5a demonstrates the orientation of the camera and the Figure 5b shows the influence of each physical displacement component from the surface on the displacement observed by the camera. In this case, off-axis 2D DIC effectively converted the pixel intensities of the video from the single camera, $I(x,y,t)$, to a 2D surface displacement video ($u(x,y,t)$, $v(x,y,t)$). Like with 3D DIC, a subset size of 21 × 21 pixels was selected with a step size of 7 pixels. Since there is no need for computationally intensive subset matching between image pairs like required by 3D DIC, the processing time was reduced by a factor of approximately three.

For 2D DIC, the damage images are the norm of the TWE of each x- and y-directional velocity component:

$$I_{2D\ DIC}(x,y) \equiv \sqrt{|\mathrm{TWE}_x(x,y)|^2 + \left|\mathrm{TWE}_y(x,y)\right|^2} \tag{2}$$

where the product of the displacement and angular frequency during the sweep was once again used as the signal in the formation of the TWE.

The damage imaging results produced from the displacement data extracted using off-axis 2D DIC are presented in Figure 4. These results closely mirror the 3D DIC results. Though there is slightly less contrast in the damaged region, this is expected since only a portion of the transverse displacement was captured. Overall, these images verify that off-axis imaging can be used to produce clear damage images of BVID with only one camera.

IMAGE DECORRELATION

Following the verification of the off-axis imaging method for capturing BVID, image decorrelation was explored as a replacement for DIC to reduce data processing time. The decorrelation value describes the pixel intensity change from surface movement and is scalar. While the sensitivity of decorrelation at each pixel will depend heavily on the speckle pattern content within, the apparent surface movement is influenced by $\cos(\theta)$ of the x-displacement, all the y-displacement, and $\sin(\theta)$ of the z-displacement, equivalent to the norm of the vectors described in Figure 5b.

After images were captured and saved in TIFF format, they were imported directly into MATLAB for off-axis video frame decorrelation. To make it possible to import the images into MATLAB for processing and to make the data size more manageable, images were all spatially downsampled by averaging groups of four pixels together. Images were also divided into two groups (even and odd) and processed separately to further reduce the import size. Images from each group were averaged together to produce the final damage image. This reduced the number of images that needed to be imported at one time to 9600 and lowered the effective frame rate to 3.2 kHz.

To extract the magnitude of surface change across each frame, the normalized cross-correlation (NCC) was selected as the decorrelation algorithm since it is invariant to global changes in intensity, like lighting changes between two images, and the normalization step generally makes it more robust [16]. For localization across the image, the decorrelation was calculated using a sliding window of size $N \times N$. The following formulation for the local NCC using this sliding window is:

$$NCC_{uv}(d,r) = \frac{\sum_{x=u}^{u+N-1}\sum_{y=v}^{v+N-1}[d(x,y)-\mu_{d,(uv)}][r(x,y)-\mu_{r,(uv)}]}{\sqrt{\sum_{x=u}^{u+N-1}\sum_{y=v}^{v+N-1}[d(x,y)-\mu_{d,(uv)}]^2}\sqrt{\sum_{x=u}^{u+N-1}\sum_{y=v}^{v+N-1}[r(x,y)-\mu_{r,(uv)}]^2}} \quad (3)$$

where N is the length of the square window, (u, v) are the coordinates of the window origin, $d(x, y)$ is the displaced image, $r(x, y) = \frac{1}{N^2}\sum_{f=1}^{F} D(x, y, f)$ is the reference image equal to the temporal mean over all frames for each pixel, $\mu_{d,(uv)}$ is the spatial mean of the window in the displaced image, and $\mu_{r,(uv)}$ is the spatial mean of the window of the reference image. As applied in this work, decorrelation effectively converted the pixel intensities of the video from the single camera, $I(x,y,t)$, to an array of scalar decorrelation values, $NCC(x,y,t)$. For this study, a window size of $N = 11$ and a step size of 4 pixels were chosen for NCC to provide a balance for the best damage visibility. After accounting for downsizing, this corresponds to the subset

size of 21 and step size of 7 used for DIC. An optical axis angle of $\theta = 22°$ relative to the surface normal was selected as a balance between capturing the resonance with adequate intensity and reducing fringe pattern artifacts created by pixels either sampling the edges of speckles (high sensitivity to movement) or nearly solid white or black regions (low sensitivity). This direct, pixel-by-pixel, method of extracting surface dynamics does not require any subset matching, reducing the total processing time by approximately 5 times compared to 2D DIC and 15 times compared to 3D DIC.

For image decorrelation, the damage images are equivalent to the TWE of the decorrelation map:

$$I_{decorr}(x, y) \equiv \mathrm{TWE}_{NCC}(x, y) \tag{4}$$

where the product of the decorrelation value and angular frequency during the sweep was used in this case as the signal in the formation of the TWE. A 0.2 kHz high pass filter was applied directly to the video before computing the TWE.

The damage images produced from the displacement data extracted using NCC image decorrelation are presented in Figure 4. All damage images of Panel A are very similar to those produced using DIC. Like with DIC, the discrepancy in the clarity of images from Panel A and B is likely due to less energy being captured damage region in Panel B, reducing the scale (note the maximum scale value) to make artifacts and noise more apparent. While the artifacts in the Panel B images produced with DIC were around the corners and likely caused by increased subset matching uncertainty in regions of poorer focus and lighting conditions due to the oblique optical axis, the artifacts in the images produced with image decorrelation are within the center and likely due to the fringe patterns described earlier. Despite these artifacts, the damage region clearly stands out from the rest of the FOV, and the signal-to-noise ratio is comparable to those in the images from 2D DIC and 3D DIC.

CONCLUSIONS

In this work, an efficient and reliable computer vision-based system for inspection (NDI) or monitoring (SHM) was developed to visualize hidden impact damage in composite structures. Specifically, the technique for extracting surface dynamics from images was optimized by employing a single camera to image BVID in composites and using an efficient image decorrelation algorithm for extraction to skip the computationally intensive subset matching required by DIC. Overall, the damage images formed by the TWE imaging condition based on the decorrelation values provide baseline-free damage identification since the reference state is determined by the temporal mean of all frames. Thus, the proposed computer-vision-based method is robust, efficient, and has a high potential for in-time inspection of critical composite structures with additional development. Since the image decorrelation technique relies on the grayscale intensity changes, the sensitivity of the decorrelation algorithm could be further improved by using a camera with a higher bit depth, and the SNR could be improved by acquiring more images during the sweep by using a camera with a higher frame rate and memory. While the time required for processing has been significantly reduced compared to previous efforts,

the practicality of the work is still limited by the need to apply an artificial speckle pattern to the surface. Future work will focus on using a projected speckle pattern, rather than an applied speckle pattern, with the decorrelation technique to avoid the need for surface preparation.

ACKNOWLEDGEMENTS

The author, T. Bryce Abbott, is grateful for the support from North Carolina Space Grant and the National Institute of Aerospace (NIA), Hampton, Virginia.

REFERENCES

1. V. Giurgiutiu and C. Soutis. 2012. "Enhanced composites integrity through structural health monitoring," *Applied Composite Materials*, 19:813-829.
2. S. Sanchez-Saez, E. Barbero, R. Zaera, and C. Navarro. 2005. "Compression after impact of thin composite laminates," *Compos Sci Technol*, 65(13):1911-1919.
3. T. S. Lim, C. S. Lee, and D. G. Lee. 2004. "Failure modes of foam core sandwich beams under static and impact loads," *J Compos Mater*, 38(18): 1639-1662.
4. C. Z. Dong and F. N. Catbas. 2021. "A review of computer vision–based structural health monitoring at local and global levels," *Structural Health Monitoring*, 20(2):692-743.
5. B. F. Spencer, V. Hoskere, and Y. Narazaki. 2019. "Advances in Computer Vision-Based Civil Infrastructure Inspection and Monitoring," *Engineering*, 5(2):199-222.
6. L. Tian, T. Ding, and B. Pan. 2022. "Generalized Scale Factor Calibration Method for an Off-Axis Digital Image Correlation-Based Video Deflectometer," *Sensors*, 22(24):10010.
7. B. Pan. 2018. "Digital image correlation for surface deformation measurement: Historical developments, recent advances and future goals," *Meas Sci and Technol*, 28(8):082001.
8. M. A. Sutton, F. Matta, D. Rizos, R. Ghorbani, S. Rajan, D. H. Mollenhauer, H. W. Schreier, and A. O. Lasprilla. 2017. "Recent Progress in Digital Image Correlation: Background and Developments since the 2013 W M Murray Lecture," *Exp Mech*, 57(1):1-30.
9. V. Giurgiutiu. 2006. *Structural health monitoring with piezoelectric wafer active sensors*. Elsevier.
10. H. Y. Chang and F. G. Yuan. 2020. "Visualization of hidden damage from scattered wavefield reconstructed using an integrated high-speed camera system," *Struct Health Monit*, 20(5):2300-2316
11. T. B. Abbott and F. G. Yuan. 2023. "Subsurface Impact Damage Imaging for Composite Structures using 3D DIC," *Struct Health Monit*.
12. D. M. Tsai and C. T. Lin. 2003. "Fast normalized cross correlation for defect detection," *Pattern Recognit Lett*, 24(15): 2625-2631.
13. F. A. Leone Jr, D. Girolamo, and C. G. Davila. 2012. "Progressive damage analysis of bonded composite joints," No. NASA/TM-2012-217790.
14. P. Reu. 2014. "All about speckles: Aliasing," *Exp Tech*, 38(5): 2014, 38(5):1-3
15. "VID-3D – Correlated Solutions Digital Image Correlation," Retrieved from *https://www.correlatedsolutions.com/vic-3d/*. Accessed Sept 28, 2022.
16. J. van Welzen, F.-G. Yuan, and R. Y. Fong. 2021. "Comparison of image correlation algorithms for hidden damage laser speckle photometry," *Sensors and Smart Structures Technologies for Civil, Mechanical, and Aerospace Systems*, *SPIE*, 11591:132-151.